Deformation and exhumation of the Ronda peridotite (Spain)

Jacques Précigout, Frédéric Gueydan, Carlos J Garrido, Nathan Cogné, Guillermo Booth-Rea

Deformation and exhumation of the Ronda peridotite (Spain)

Jacques Précigout,[1] Frédéric Gueydan,[2] Carlos J. Garrido,[3] Nathan Cogné,[4] and Guillermo Booth-Rea[5]

Received 5 November 2012; revised 5 May 2013; accepted 26 June 2013; published 4 August 2013.

[1] The Ronda peridotite supplies one of the best objects to document subcontinental mantle deformation, but its internal deformation and exhumation mechanisms remain controversial. Here we provide new structural data and numerical results that constrain the Oligocene-Miocene deformation history of the Ronda massif. We first describe a mantle shear zone in the northern massif that developed subcrustal strain localization during decompression and related partial melting. The deformation regime of this mantle shear zone evolved from penetrative NE-SW stretching to sinistral shear highlighted by discrete shear bands. We then show structural observations that document a viscous deformation in the southern massif occurring prior to the thrust-assisted emplacement of the peridotite during large decompression. Finally, we performed numerical investigations that quantify a high temperature of 980°C for the basal peridotite lens at the time of its crustal emplacement. Our numerical results constrain the timing of ductile deformation of the peridotite just before 22 Ma, probably between 30 and 22 Ma. Altogether, these features led us to conclude that the deformation and exhumation of the Ronda peridotite results from lithosphere thinning subsequently inverted in the course of the Oligocene-Miocene. Among available models, our findings support the hypothesis of peridotite exhumation by the inversion of a thinned back-arc continental lithosphere during westward slab rollback through the Alboran region.

Citation: Précigout, J., F. Gueydan, C. J. Garrido, N. Cogné, and G. Booth-Rea (2013), Deformation and exhumation of the Ronda peridotite (Spain), *Tectonics*, *32*, 1011–1025, doi:10.1002/tect.20062.

1. Introduction

[2] Deformation of the subcontinental mantle strongly affects the mechanics of the continental lithosphere and, somehow, the tectonic processes at the Earth's surface. Natural documentations of mantle structures are thus crucial to account for the lithosphere dynamics. In mountain belts, the presence of subcontinental peridotites is frequently described, but their restricted sizes strongly limit the amount of information, especially for structural features that often need map-scale observations to be exhaustively documented. The Ronda peridotite in southern Spain exposes the largest outcrop of subcontinental mantle in the world (300 km^2) [*Obata*, 1980]. It thus gives one of the best opportunities to thoroughly describe subcontinental deformation. However, several conflicting models have been proposed to account for the deformation and exhumation of the Ronda massif, and they do not provide any consensus to objectively interpret the structural features of the Ronda peridotite.

[3] Depending on the model, the tectonic context of the Ronda massif involves either (1) a mantle core complex [*Doblas and Oyarzun*, 1989], (2) the extrusion of a mantle wedge during transpression [*Tubía et al*., 2004, 2012; *Mazzoli and Algarra*, 2011], (3) the succession of detachment faults during extensional collapse of the Betic-Rif chain [*Van der Wal and Vissers*, 1993; *Platt et al*., 2003b], or (4) the inversion of a thinned back-arc lithosphere during slab rollback-related subduction of the Iberian passive margin [*Booth-Rea et al*., 2005; *Garrido et al*., 2011]. At present, although some models have been discarded, the exhumation process of the Ronda peridotite is still highly debated.

[4] In this paper, we first propose to discuss the available data about the deformation affecting both the Ronda peridotite and its crustal envelope. We then expose new structural documentations of the western massif that better constrain the deformation conditions of the peridotite. We also show new results of numerical thermal investigations concerning the peridotite tectonic emplacement, which put further constraints on the timing of the Ronda peridotite deformation.

[1]Institut des Sciences de la Terre d'Orléans, Université d'Orléans, Orléans, France.
[2]Géosciences Montpellier, Université de Montpellier 2, Montpellier, France.
[3]Instituto Andalouz de Ciencias de la Tierra, CSIC, Facultad des Ciencias, Granada, Spain.
[4]Department of Geology, Trinity College Dublin, University of Dublin, Dublin, Ireland.
[5]Departamento de Geodynámica, Facultad de Ciencias, Universidad de Granada, Granada, Spain.

Corresponding author: J. Précigout, Institut des Sciences de la Terre d'Orléans, INSU-CNRS-Université d'Orléans, Campus Géosciences, 1A rue de la Férollerie, FR-45071 Orléans CEDEX 2, France. (jacques.precigout@univ-orleans.fr)

0278-7407/13/10.1002/tect.20062

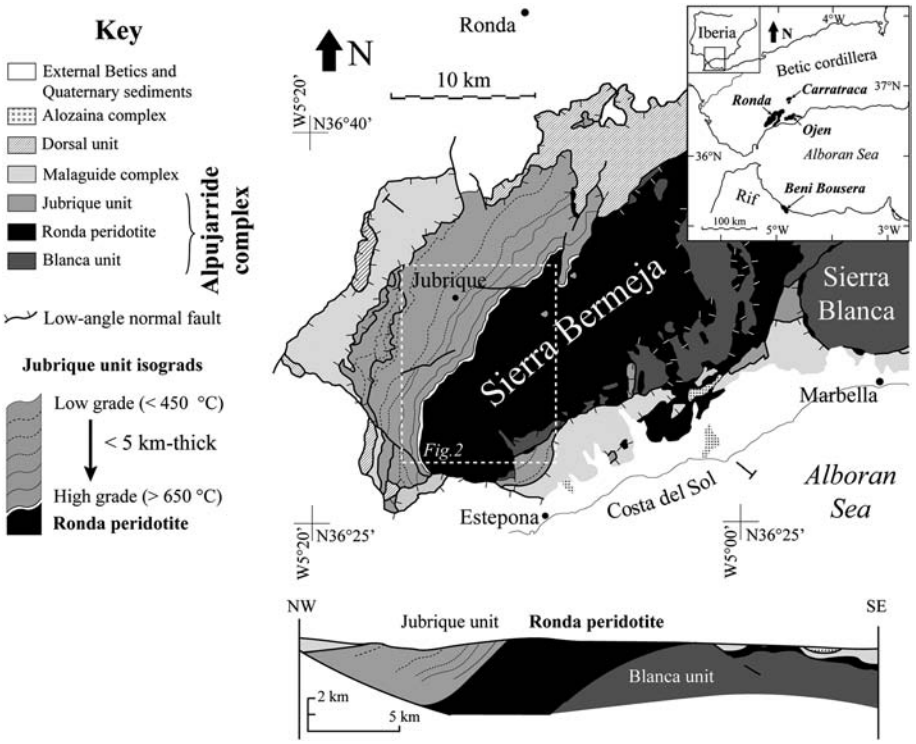

Figure 1. Location, map, and cross section of the Ronda peridotite (map modified after *Sanchez-Gomez et al*. [2002]; cross section modified after *Garcia-Dueñas et al*. [1992]). The metamorphic isograds of the Jubrique unit have been also shown [*Sanchez-Gomez et al*., 2002].

Finally, based on existing models, we discuss the tectonic context of the Ronda peridotite and propose a new model of deformation and exhumation.

2. Geological Setting

2.1. The Betic-Rif Chain

[5] The Ronda peridotite belongs to the Betic cordillera in southern Spain, which composes the Gibraltar arc with the Rif Mountains in northern Morocco (Figure 1, inset). The external domain of this arc-shaped ridge shows a fold-and-thrust belt composed of the Mesozoic and Tertiary sediments of the Iberian and Moroccan paleomargins [*Platt et al*., 2003a, and references therein]. In the inner part that borders the Alboran Sea, Paleozoic and Mesozoic metamorphosed sediments of the Alboran domain overlie the external domain and compose the internal Betics and Rif [*Andrieux et al*., 1971]. A fold-and-thrust belt of Cretaceous to Miocene flysch-type sediments also occurs between these external and internal domains in the western end of the Betic-Rif chain [e.g., *Balanyá and Garcia-Dueñas*, 1987; *Luján et al*., 2000, 2006].

[6] The internal Betics expose three nappe complexes, from bottom to top: (1) the Nevado-Filábride complex that recorded variable degrees of metamorphism from high pressure/low temperature to low pressure (LP)/high temperature (HT) during the Miocene [*Puga et al*., 1999; *Augier et al*., 2005; *Platt et al*., 2006], (2) the Alpujarride complex that also recorded variable metamorphic conditions from high pressure/low temperature during the late Eocene–Oligocene to LP/HT during the Oligocene–early Miocene [*Balanyá et al*., 1997; *Azañon and Crespo-Blanc*, 2000; *Azañon and Goffé*, 2005; *Rossetti et al*., 2005; *Platt et al*., 2005, 2006], and (3) the Malaguide complex that only recorded very low grade metamorphism [*Lonergan*, 1993].

[7] The Ronda peridotite, in a broad sense, encompasses three main peridotite massifs: Ronda, in a strict sense, Ojen, and Carratraca (Figure 1, inset). They all occur as peridotite lenses within the high-grade metamorphic crust of the upper Alpujarride [*Tubía et al*., 1992], but they should also extend offshore as suggested by the gravimetric anomalies along the Iberian and Moroccan coasts [*Torné et al*., 1992]. We focus our study on the western part of the Ronda peridotite (Figure 1).

2.2. The Crustal Envelope

[8] In northwestern Sierra Bermeja, a sequence of continental crust (Jubrique unit) overlies the Ronda peridotite (Figure 1) [*Balanyá et al*., 1997]. This metapelitic unit belongs to the upper Alpujarride and displays a metamorphic imprint that grades from medium pressure/high temperature in felsic granulite facies (kinzigites) at the contact with the peridotite to low pressure/low temperature in phyllites below the low-grade Malaguide complex. From bottom to top—and lying between the kinzigites and phyllites—migmatites, gneisses, and schists occur structurally parallel to the northern contact of the peridotite [*Balanyá et al*., 1997; *Negro et al*., 2006]. In addition, petrological investigations described a strongly decompressive *P-T* path for all units and yielded metamorphic ages between 19 and 23 Ma [*Priem et al*., 1979; *Balanyá et al*., 1997; *Platt et al*., 2003b]. Based on these features and the strong metamorphic gradient through the crustal sequence (Figure 1) [*Balanyá et al*., 1997; *Sanchez-Gomez et al*., 2002; *Negro et al*., 2006], *Tubía et al*. [1993],

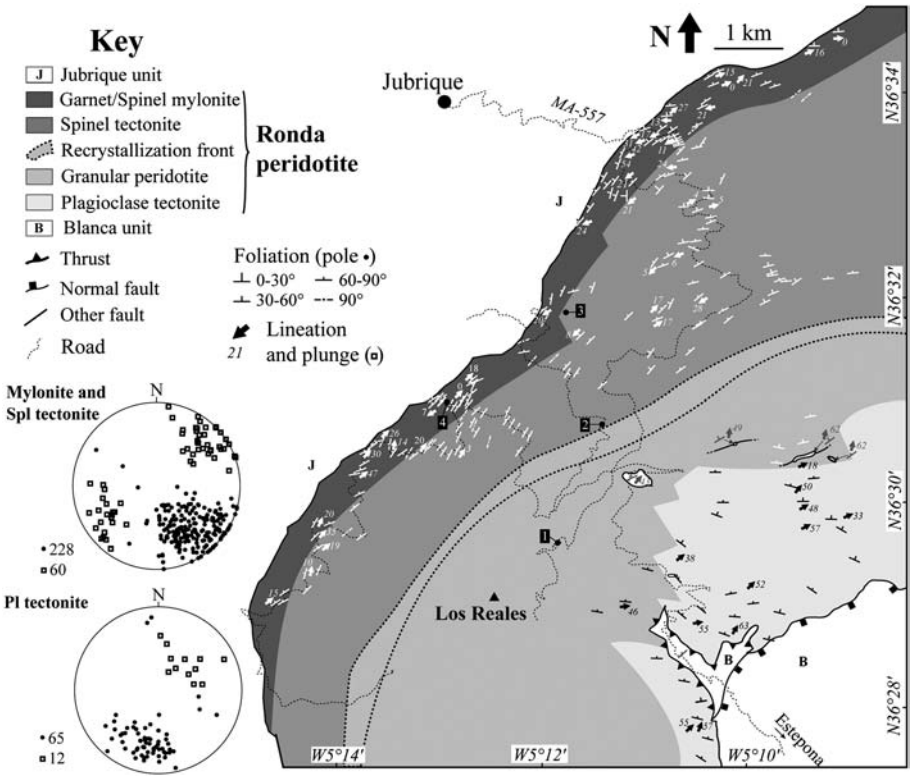

Figure 2. Structural map of the western Ronda peridotite. The domain boundaries are from *Van der Wal and Vissers* [1996] and *Lenoir et al*. [2001]. Stereograms for foliation and lineation data are presented in equal-area, lower-hemisphere projections. Numbers on the map indicate locations of pictures in Figure 5.

Balanyá et al. [1997], and *Argles et al*. [1999] related the main deformation of the Jubrique unit to intense thinning of a continental crust during the Oligocene–early Miocene. *Balanyá et al*. [1997], moreover, showed a conspicuous structural consistency between the basal Jubrique crustal units and the intense deformation (mylonite) on top of the peridotite.

[9] Farther to the south and to the east, metapelitic rocks underlie the Ronda peridotite. They have been described as belonging to the Blanca unit (Figure 1) [*Tubía et al*., 1992]. Both deformation and partial melting atop of this unit have been related to the top-to-the-north "hot" emplacement of the Ronda peridotite onto continental crust [*Westerhof*, 1977; *Lundeen*, 1978; *Tubía et al*., 1997; *Esteban et al*., 2004, 2008], which formed a so-called dynamothermal aureole [*Tubía et al*., 1997]. Partial melting produced leucocratic felsic dykes that intruded both the peridotite and the overlying Jubrique unit. Rb/Sr and K/Ar analyses in biotite permitted dating these dykes and the dynamothermal aureole at 22 ± 4 and 18.8 ± 4.9 Ma, respectively [*Loomis*, 1975; *Priem et al*., 1979; *Cuevas et al*., 2006]. More recently, U/Pb sensitive high-resolution ion microprobe dating has yielded ages of 22.3 ± 0.7 Ma for the dynamothermal aureole and 22.6 ± 1.8 and 21.5 ± 3.8 Ma for the granitic dykes [*Esteban et al*., 2011], constraining the emplacement of the Ronda peridotite around 22 Ma ago. The south edge of the Ronda peridotite is also marked by large-scale normal faults that extend eastward along strike. This brittle deformation has been attributed to the Miocene extensional event that led to the final exhumation of the Alpujarride crust in the internal Betics [*Rossetti et al*., 2005, and references therein]. In relation to that, *Monié et al*. [1994], *Platt et al*. [2003b], and *Esteban et al*. [2004] described a high cooling rate (300°C/Ma to 100°C/Ma) between 21 and 17 Ma of all crustal rocks that surround the Ronda peridotite.

3. The Ronda Peridotite

3.1. Petrostructural Domains

[10] Several studies have described in detail the western Ronda peridotite [*Obata*, 1980; *Van der Wal and Vissers*, 1993, 1996; *Van der Wal and Bodinier*, 1996; *Garrido and Bodinier*, 1999; *Lenoir et al*., 2001; *Précigout et al*., 2007; *Soustelle et al*., 2009; *Garrido et al*., 2011]. In this area, four structural-petrological-geochemical domains occur, from top to bottom: a garnet (Grt)/spinel (Spl) mylonite domain, a Spl tectonite domain, a Spl coarse granular peridotite domain, and an underlying plagioclase (Pl) tectonite domain (Figure 2) [*Van der Wal and Vissers*, 1996].

[11] Both the Grt/Spl mylonite and the Spl tectonite are composed of variably serpentinized lherzolite, harzburgite, and minor dunite. They show a penetrative foliation with a strike and dip of roughly N50°, 80°NW, which becomes progressively more penetrative from the tectonite toward the mylonite, mainly across the mylonite (Figures 3a and 3b). Throughout these two domains, the stretching lineation is nearly horizontal, and previous studies documented a combination of sinistral kinematics [*Van der Wal and Vissers*, 1996] and NE-SW penetrative stretching without clear kinematics [*Balanyá et al*. 1997; *Argles et al*., 1999]. These domains are also interlayered by garnet-bearing pyroxenites (group A pyroxenites of *Garrido and Bodinier* [1999]), where garnets are usually surrounded by undeformed kelyphite

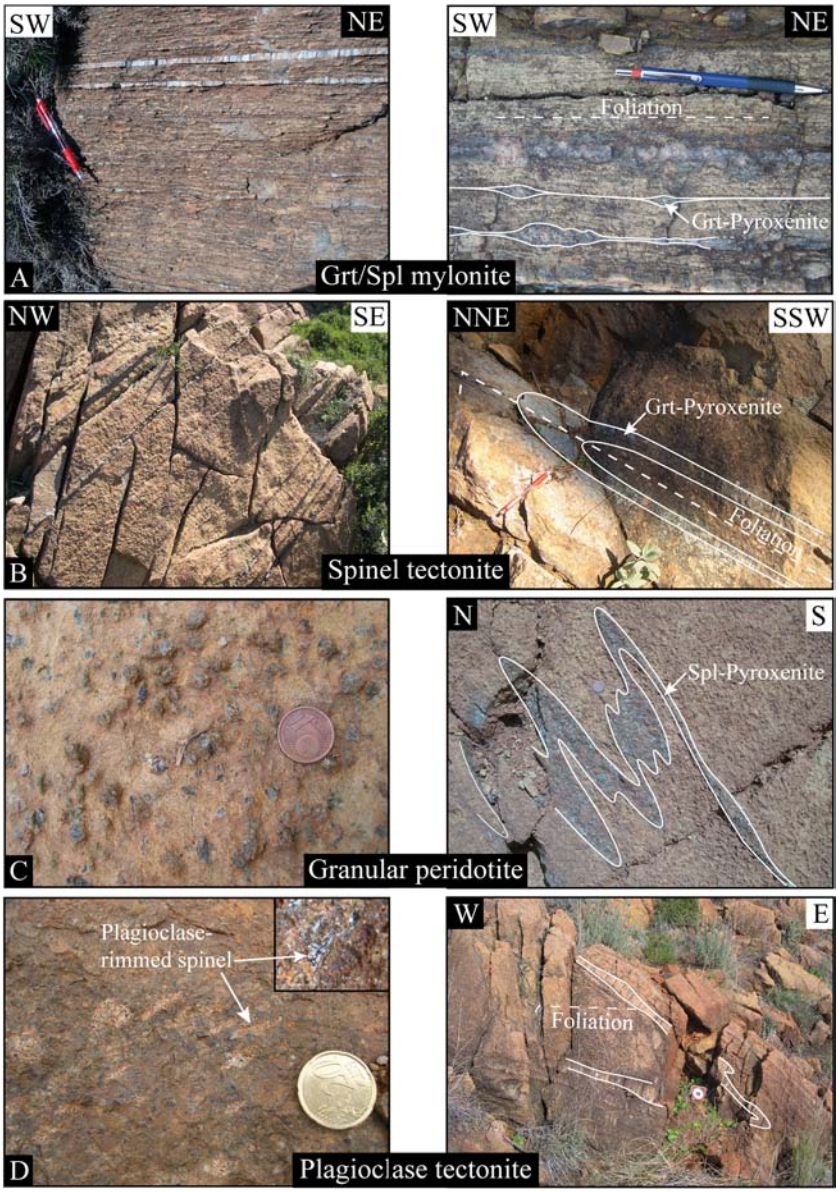

Figure 3. (a) Penetrative foliation and pinch-and-swell structures of Grt-bearing pyroxenite in the Grt/Spl mylonite. (b) Penetrative foliation and isoclinal fold of pyroxenites layers in the Spl tectonite. The foliation (dashed line) lies parallel to the axial plane of folds. (c) Granular aspect and pyroxenite fold in the granular peridotite domain. (d) Foliation and meter-scale fold of pyroxenite in the plagioclase-bearing domain. The inset shows the subsolidus plagioclase around spinel. The obliquity between the foliation and the axial plane of the pyroxenite fold shows that the ductile deformation of the plagioclase tectonite postdates the meter-scale folding.

formed at low pressure (4–8 kbar) [*Obata*, 1994; *Van der Wal and Vissers*, 1996]. In the Spl tectonite, garnet-bearing pyroxenites are transposed and lie parallel to the Spl tectonite foliation. They are generally straight but locally show boudins and isoclinal folds with their axes oriented NE-SW slightly dipping toward the NE (Figure 3b) [*Garrido and Bodinier*, 1999]. In the Grt/Spl mylonite, pyroxenite layers are strongly stretched, as shown by pinch and swell types of boudinage (Figure 3a). In these pyroxenites, while Lu/Hf isochron and Th/U dating indicate variable ages between 300 ± 8 and 88.6 ± 3.1 Ma in the core of zircon, some dating at their rim yielded metamorphic ages between 22.8 ± 1.8 and 25 ± 0.9 Ma [*Blichert-Toft et al.*, 1999; *Sanchez-Rodriguez and Gebauer*, 2000]. Some garnets also occur in peridotites that surround these Grt-bearing pyroxenites, but only for highly strained peridotites that lie just beneath the crustal rocks of Jubrique [*Obata*, 1980]. At places, highly strained boudins of garnet-bearing pyroxenite contain garnet porphyroclasts in their core. Some of these pyroxenites preserved rare graphitized diamonds that attest of the deep origin of these mantle rocks (>150 km) [*Davies et al.*, 1993; *Pearson et al.*, 1995]. The contact between the Grt/Spl mylonite and the overlying Jubrique unit is highly tectonized and serpentinized.

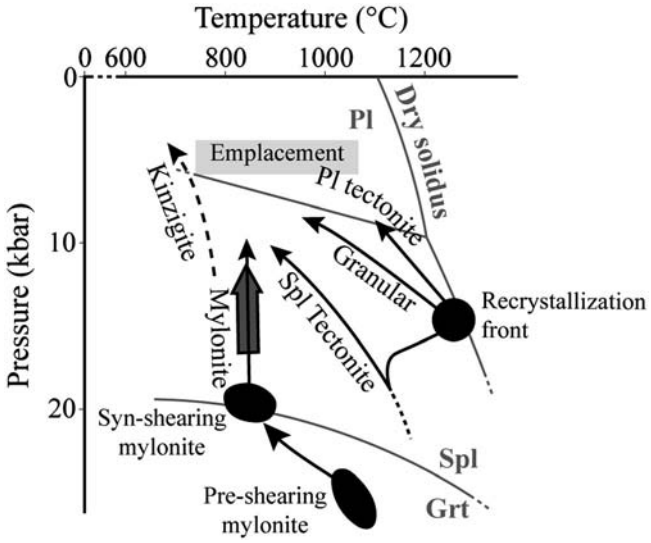

Figure 4. Pressure-temperature (*P-T*) path of the Ronda peridotite. Data and *P-T* paths are from *Morishita et al*. [2001] (dark gray arrow), *Lenoir et al*. [2001] (recrystallization front), *Esteban et al*. [2008] (emplacement of the peridotite), *Garrido et al*. [2011](pre-shearing and syn-shearing mylonite), and *Balanyá et al*. [1997] (kinzigite). We also proposed hypothetic *P-T* paths for the Spl tectonite and granular domains based on the data set from *Garrido et al*. [2011]. Pressure-temperature fields of garnet (Grt), spinel (Spl), and plagioclase (Pl) are from *Garrido et al*. [2011].

[12] The coarse granular peridotite domain, underlying the Spl tectonite domain, is composed of spinel harzburgite with minor lherzolite and dunite [*Lenoir et al*., 2001] interlayered with numerous Spl-bearing pyroxenites (Figure 3c) (group B and C of *Garrido and Bodinier* [1999]). The transition with the overlying Spl tectonite is a relatively sharp 400 m wide zone characterized by a sudden increase in grain size of the peridotite minerals [*Vauchez and Garrido*, 2001]. Across this so-called recrystallization front, from the Spl tectonite to the granular peridotite, the tectonic foliation in the peridotite disappears (Figure 3c), and garnet breaks down to spinel in the pyroxenite layers (group B of *Garrido and Bodinier* [1999]). Based on the strike-and-dip consistency between the spinel pyroxenite layers in the granular domain and the garnet pyroxenite layers in the Spl tectonite, *Van der Wal and Bodinier* [1996] proposed that coarse-grained peridotites resulted from "static" coarsening/annealing of the basal Spl tectonite peridotites. The presence of meter-scale isoclinal folds of Spl pyroxenite (Figure 3c) and the preservation of a strong olivine lattice preferred orientation (LPO) both support this tectonite-related deformation in the seemingly undeformed granular peridotite [*Garrido and Bodinier*, 1999; *Vauchez and Garrido*, 2001; *Soustelle et al*., 2009].

[13] Farther to the south, the Pl-bearing domain is marked by the appearance of a penetrative foliation in lherzolite and a less penetrative foliation in harzburgite and dunite. The foliation shows a strike and dip of about N110°, 60°N and bears a N45°, 45°N lineation direction and plunge (Figure 2). The occurrence of subsolidus plagioclase around spinel, mostly for lherzolitic bulk compositions [*Bodinier et al*., 2008], also characterizes this domain (Figure 3d). Furthermore, all the peridotites are layered by Spl/Pl pyroxenites, which are affected by metric and hectometric folding. While hectometric folds are related to the penetrative deformation of the plagioclase tectonite—they show axial planes parallel to the plagioclase-bearing foliation [*Van der Wal and Vissers*, 1996]—metric folds are structurally inconsistent with the deformation of the plagioclase tectonite (Figure 3d). Several hectometric bodies of quartz-feldspar mylonites, migmatites, and marbles from the Blanca unit also occur in both the Pl tectonite and the granular peridotite domains. These bodies contain a rather constant internal foliation of N50°, 60°NW and are bounded by brittle faults that crosscut the foliation of the Pl tectonite. They represent crustal imbrications that were tectonically incorporated into the peridotite [*Sanchez-Gomez et al*., 2002]. In addition, numerous late outcrop- and map-scale normal brittle faults occur throughout the Ronda massif.

3.2. Pressure-Temperature Path

[14] The *P-T* path of the Ronda peridotite remains a matter of debate, and some data are only available for the Grt/Spl mylonite and the granular peridotite. In terms of pressure, the Ronda *P-T* path shows decompression from deep lithosphere to midcrustal depths for all units composing the massif (Figure 4) [*Garrido et al*., 2011]. In a previous study, *Van der Wal and Vissers* [1993] involved an increase in pressure during former deformation in the mylonitic domain, but they based their interpretation on the occurrence of garnet-rimmed spinel in the upper mylonite. *Garrido et al*. [2011] have recently shown that these garnets do not represent pressure-indexing minerals but, instead, would be due to strain-induced processes during mylonitization. They, moreover, documented decompression from pre-shearing conditions at 24–27 kbar to syn-shearing conditions around 20 kbar. Furthermore, *P-T* calculations in lenses of mafic granulites within the Grt/Spl mylonite indicate that mylonitization only recorded decompression from 18 to 10 kbar [*Morishita et al*., 2001]. Altogether, these features suggest that the Ronda mylonite only suffered syn-tectonic decompression that probably occurred up to between 4 and 6 kbar, the pressure related to the thrust-assisted peridotite emplacement (Figure 4) [*Esteban et al*., 2008]. A similar conclusion has been recently proposed for the Grt/Spl mylonite in the Beni Bousera peridotite, structural equivalent of the Ronda massif in the Rif orogen [*Afiri et al*., 2011].

[15] In terms of temperature, both the Grt/Spl mylonite and the Spl tectonite recorded cooling, while the granular domain and the Pl tectonite suffered an increase in temperature above the peridotite solidus before to suffer subsequent cooling as well [*Van der Wal and Vissers*, 1996; *Lenoir et al*., 2001]. Note that the metapelitic envelope of Jubrique recorded a similar *P-T* path to the Ronda peridotite, with combined decompression and cooling. However, syn-kinematic pressure records indicate a gap of more than 10 kbar between the peridotite (decompression from 18 to 10 kbar) [*Garrido et al*., 2011] and the overlying kinzigite (decompression from 10 to 4 kbar) (Figure 4) [*Balanyá et al*., 1997]. This feature strongly suggests that part of the peridotite exhumation has been accommodated by the faulted crust/mantle contact as proposed by *Platt et al*. [2003b] and *Afiri et al*. [2011].

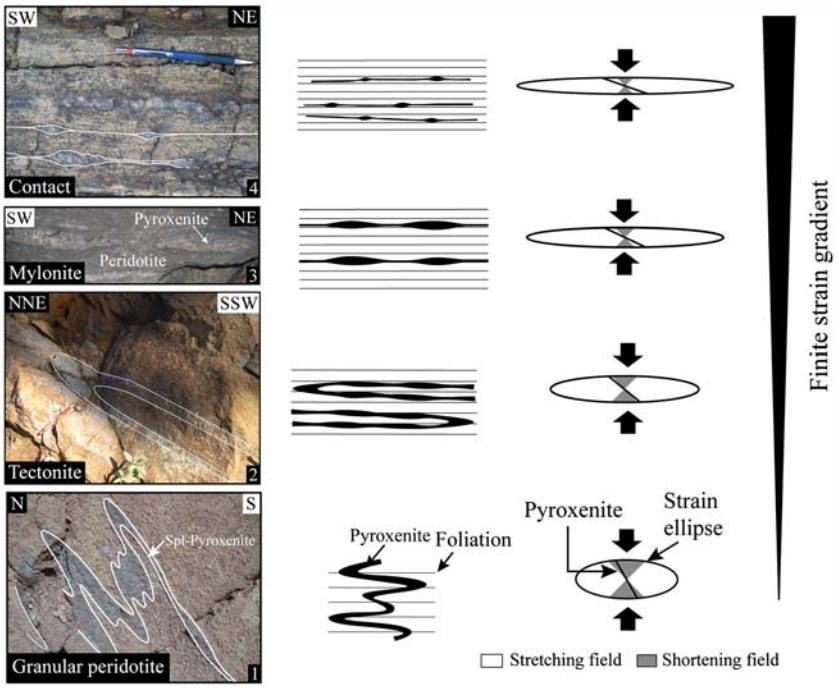

Figure 5. Deformation pattern of meter-scale pyroxenites from the granular peridotite to the Grt/Spl mylonite. This evolution describes, from steps 1 to 4 (pictures are located in Figure 2), a change in deformation pattern of passive lines (pyroxenites) from shortening (folding) to stretching (boudinage) fields with increasing ductile strain of peridotites. See text for further explanations.

4. New Structural Data

4.1. The Ronda Mantle Shear Zone

4.1.1. Strain Gradient Through the Pyroxenite Layers

[16] Numerous pyroxenite layers occur through the Ronda peridotite. They show different patterns of deformation, including boudins and metric folds in the Grt/Spl mylonite and the Spl tectonite, respectively. Some folds also occur in the granular domain. These folds developed axial planes parallel to the Spl-bearing foliation, and hence, they are contemporaneous to the Spl tectonite deformation [*Van der Wal and Vissers*, 1996; *Précigout et al*., 2007]. We thus used the deformation pattern of meter-scale pyroxenites as an indicator of strain intensity through the granular peridotite, the Spl tectonite, and the Grt/Spl mylonite (Figure 5). We excluded the meter-scale folds of the Pl tectonite because of their remobilization during deformation of this domain. With decreasing distance from the contact with the peridotite-overlying Jubrique unit, the pyroxenite folds occur progressively as open folds, closed folds, and isoclinal folds, with their limbs being more and more stretched. Then, the folds become parallel to the foliation, and the pyroxenites evolve from weakly to highly stretched in the Grt/Spl mylonite with pinch-and-swell structures (Figure 5). This evolution is consistent with an increase in strain intensity and the transposition of the pyroxenite layers that rotate with respect to the principal strain axes from shortening to stretching fields (Figure 5) [*Ramsay*, 1982]. Together with the occurrence of foliation strengthening toward the peridotite/crust contact, this feature indicates that both the tectonite and the mylonite are affected by a large-scale strain gradient resulting from ductile strain localization beneath the crustal unit of Jubrique.

4.1.2. Map-Scale Discrete Shear Deformations

[17] The penetrative deformation of the Spl tectonite and the Grt/Spl mylonite describes NE-SW stretching that becomes more and more intense toward the peridotite/crust contact. Obliquities between the foliation and the orthopyroxene exsolution lamellae are the only observed shear criteria related to this penetrative deformation. These criteria indicate both senses of shear [*Balanyá et al*. 1997; *Argles et al*., 1999], and hence, they suggest a major component of coaxial deformation. However, we highlight here the occurrence of discrete shear bands associated with sinistral shear. They mostly occur at a regional scale, but they can be locally observed at outcrop scale and discerned through mineral alignment in thin section (Figure 6). In Figure 7a, we better document the occurrence of these discrete map-scale shear bands and show two families through the foliation trajectories across the Spl tectonite and the Grt/Spl mylonite. Indeed, trajectories describe map-scale structural planes that include (1) penetrative foliation planes (S) that occur at around N80° away from shear bands, (2) a first family of shear planes (C_I) at a low angle of the foliation and oriented N55° along strike, and (3) a second family of discrete shear planes (C_{II}) at a high angle of the foliation and oriented N15° along strike. Both families of shear planes describe a sinistral kinematics. S, C_I, and C_{II} planes can be also discerned through documentation of the foliation strikes with respect to the north within a histogram (Figure 7b). This documentation describes (1) a peak of S-type foliation density around N80°, mostly preserved in the tectonite domain; (2) a second foliation peak at N50°–N60° that only occurs in the mylonite and results from C_I shearing; and (3) a third peak at N30°–N40° that shows the foliation strikes affected by C_{II} shear planes. The latter peak is present in both the mylonite and tectonite domains.

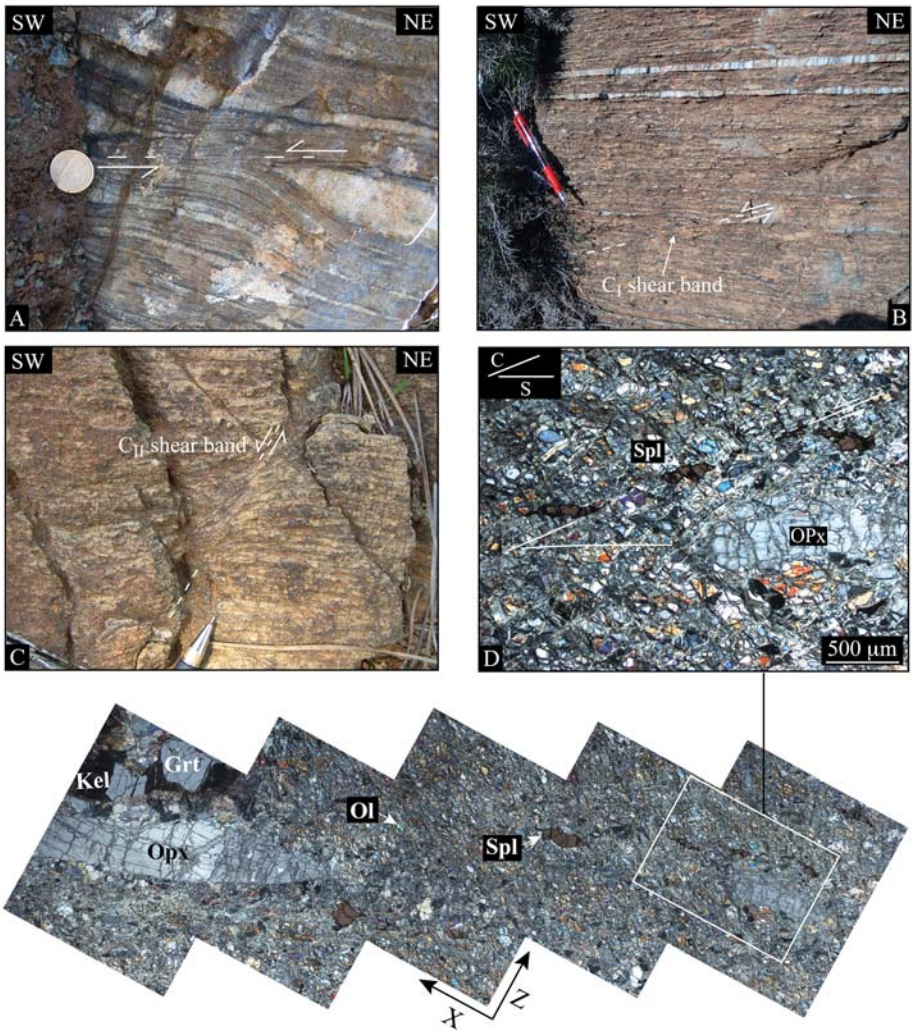

Figure 6. Outcrop-scale sinistral shear bands in the Ronda shear zone. Two types of shear bands can be observed at (a, b) a low angle and (c) a high angle of the foliation. A few low-angle shear bands are also observed in the thin section, here within (d) a Grt-bearing peridotite of the mylonite. The shear band is highlighted here by the alignment of spinel at ~30° of the foliation plane. Opx = Orthopyroxene; Spl = Spinel; Grt = Garnet; Kel = Kelyphite; Ol = Olivine.

[18] The C_I shear planes are very similar to those described by *Van der Wal and Vissers* [1996] in the "rio Guadalmanza" area close by the eastern side of our study area. In this place, they were described in the tectonite, but we show here that such C_I shear planes also occur in the mylonitic domain, where they mostly develop. The low angle between S and C_I suggests that both planes developed during progressive strain localization, producing "S-C" type structures in the peridotite mylonite [*Berthé et al*., 1979] (Figure 7). In contrast, C_{II} shear planes occur at a very high angle to S and C_I (more than 40° from C_I planes), suggesting that C_{II} planes do not represent C′ structures, which usually occur at 20° of the shear plane and result from very high strain deformation [*Berthé et al*., 1979]. Instead, they probably result from subsequent shearing that affected the whole shear zone. Note nonetheless that both C_I and C_{II} planes describe sinistral shear with close shear directions between NNE and ENE.

[19] Our observations therefore indicate that the Ronda mylonite is a remnant of a kilometer-scale mantle shear zone, which developed through a progressive strain localization process that evolved from penetrative ductile NE-SW stretching toward localized sinistral shearing in the mylonite. Then, a subsequent sinistral shear affected the whole shear zone and developed localized shear bands at ~40° of the previous shear planes.

4.2. The Granular Peridotite: Syn-tectonic Partial Melting

[20] Previous studies have shown that the granular peridotite results from partial melting of the basal Spl tectonite in asthenosphere conditions (T = 1280°C) [*Van der Wal and Bodinier*, 1996; *Lenoir et al*., 2001]. However, the timing of this partial melting with respect to the deformation of the mantle shear zone still remains a matter of debate. While *Van der Wal and Vissers* [1996] concluded that partial melting and grain coarsening postdate the deformation of the Spl tectonite, *Soustelle et al*. [2009] proposed through petrostructural and geochemical observations across the recrystallization front that partial melting affected the Spl tectonite while deforming. We show here first-order

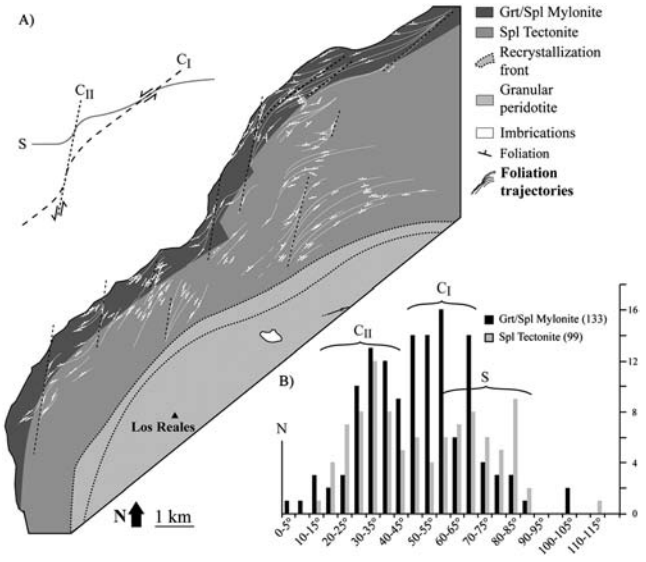

Figure 7. (a) Foliation trajectories across the Grt/Spl mylonite and Spl tectonite domains. (b) Histogram classifying the strike clockwise angles of foliation with respect to the north. We differentiate the foliation data of the mylonite from those of the tectonite (mylonite = 133 data; tectonite = 99). Both foliation trajectories and the histogram highlight map-scale sinistral shear bands that affect a foliation plane (S) oriented N80°. Two families of shear bands are observed: one at a low angle from S planes and oriented N55° (C_I) and a second one at a high angle and oriented N10°–N20° (C_{II}). While C_I shear planes describe S-C–type structures, C_{II} shear planes occur at a too high angle of C_I to be considered as C′ structures, and hence, they postdate the deformation of the Ronda shear zone (see text).

structural observations in favor of penetrative deformation in the mantle shear zone coeval with partial melting in the granular peridotite.

[21] During partial melting in the granular domain, some volatile-rich melts were produced and then infiltrated into both the Spl tectonite and the Grt/Spl mylonite, evolving subsequently as dykes of Cr-rich pyroxenite (group D pyroxenites of *Garrido and Bodinier* [1999]). These dykes can be observed in many places throughout the Ronda mantle shear zone and the granular peridotite. Close to the mylonitic domain (Figure 8), one of them lies nearly vertical and cross-cuts the Spl-bearing foliation. In the subhorizontal plane, i.e., in the plane normal to the foliation and parallel to the lineation at this place ("*X-Z*" structural plane), this Cr-rich pyroxenite dyke shows centimeter-scale folds with axial planes parallel to the foliation. This feature indicates accommodation of viscous deformation in the mantle shear zone while the pyroxenite dyke intruded it. We therefore conclude that asthenosphere-related partial melting in the granular domain was coeval with the penetrative deformation stage of the overlying mantle shear zone. The moderate amplitude of folding suggests, nevertheless, that partial melting occurred just before the end of the ductile deformation event that formed the mantle shear zone.

4.3. The Plagioclase Tectonite: Ductile Deformation Prior to Peridotite Emplacement

[22] The Ronda peridotite was tectonically emplaced onto the crust of the internal Betics (Blanca unit) during the early Miocene [*Lundeen*, 1978; *Esteban et al*., 2008]. The last viscous deformation stage of the western Ronda peridotite, now preserved in the plagioclase tectonite domain (Figure 2), has been related to this top-to-the-north emplacement stage [*Van der Wal and Vissers*, 1996]. However, we show here structural observations that question such an interpretation.

[23] In Figure 9, we show the foliation trajectories in the plagioclase tectonite based on the data set of foliation strike and dip displayed in Figure 2. Trajectories highlight progressive clockwise rotation of the foliation strike toward the major tectonic imbrication of the Blanca unit at the south edge of the peridotite massif (Figure 9). This feature indicates map-scale dextral shearing at the vicinity of the imbrication, suggesting that the development of the plagioclase-bearing foliation predates the tectonic intrusion of the "Blanca" imbrications, which is related to the peridotite emplacement [*Sanchez-Gomez et al*., 2002; *Esteban et al*., 2008]. Furthermore, shear criteria indicate inconsistent kinematics between the peridotite emplacement and the deformation of the Pl tectonite. While the emplacement occurred toward the north [*Esteban et al*., 2008], the plagioclase tectonite developed top-to-the-southwest deformation [*Van der Wal and Vissers*, 1996; *Hidas et al*., 2013].

[24] In relation to this, the development of subsolidus synkinematics plagioclase at the tip of spinel indicates that deformation occurred during decompression of the peridotite

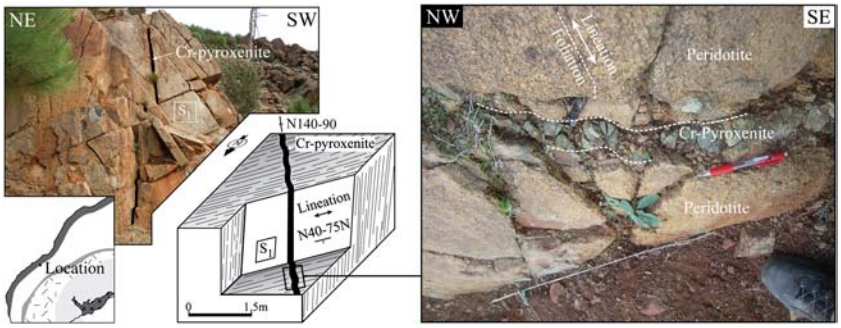

Figure 8. Chromium (Cr)-rich pyroxenite dyke intruding the mantle shear zone. In the plane normal to the foliation that contains the lineation, i.e., the subhorizontal plane at this place, the pyroxenite dyke displays some folds with axial planes parallel to the foliation, which indicates dyke intrusion during late deformation of the mantle shear zone.

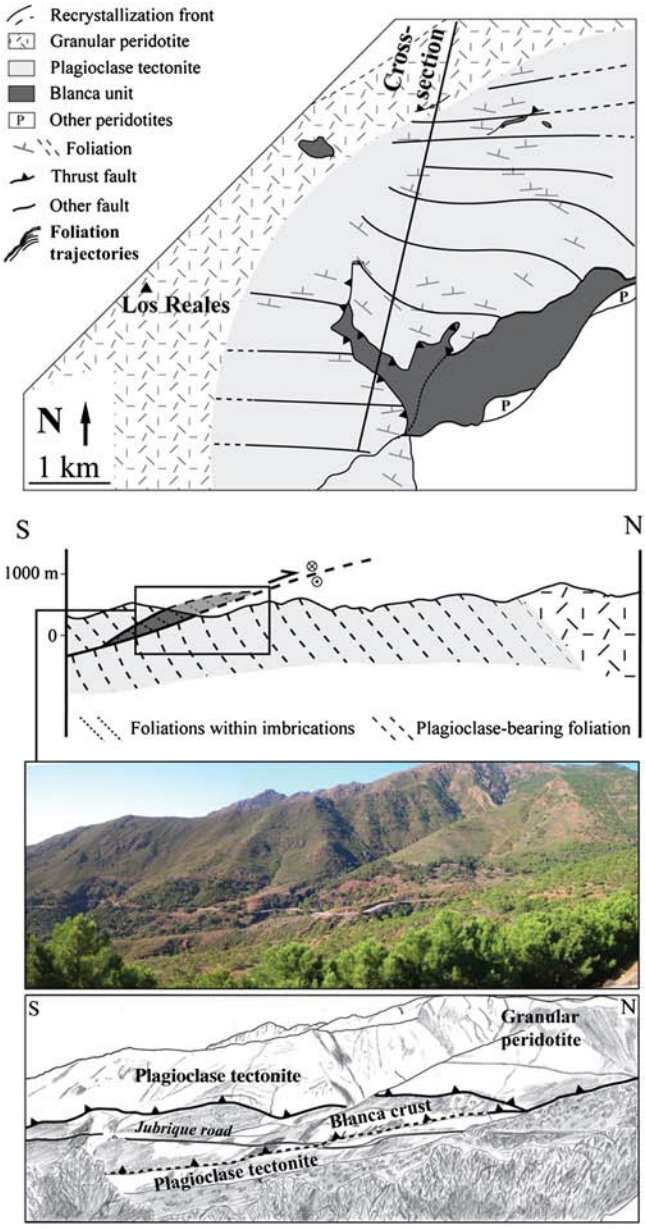

Figure 9. Foliation trajectories (map) and cross section of the plagioclase tectonite that both illustrate the occurrence of a north verging fault affecting the Pl-bearing foliation at its vicinity. This fault contains several imbrications of the peridotite-underlying Blanca unit. These features indicate that the peridotite emplacement postdates the deformation of the plagioclase tectonite (see text).

across the spinel/plagioclase boundary reaction, which lies at around 10 kbar, i.e., around 30 km depth (Figure 4). Thus, the deformation of the Pl tectonite started at a minimum depth of 30 km. Based on the pressure records of 6 kbar in crustal mylonites of the dynamothermal aureole, the base of the Ronda peridotite was at a maximum of 18 km depth during its emplacement, and hence, a stage of decompression from 30 to 18 km depth necessarily occurred before the emplacement of the Ronda peridotite. We therefore emphasize that the plagioclase tectonite probably results from viscous deformation prior to the peridotite emplacement during decompression into the plagioclase stability field.

5. Timing of Peridotite Deformation: Constraints From Thermal Modeling

[25] The ductile deformation of the Ronda peridotite implies thereby the development of a kilometer-scale mantle shear zone with coeval partial melting of its basal protolith and then a second deformation affecting part of the partially melted domain during decompression at midcrustal depth. Both events occurred prior to the tectonic emplacement of the peridotite lens around 22 Ma ago. Although the exact timing of these deformations prior to thrusting is crucial to constrain the geodynamic context of the Ronda peridotite, it remains very controversial. Indeed, previous studies have first documented late Paleozoic and Mesozoic ages between 300 and 88 Ma, which would relate the peridotite deformations to pre-Tertiary tectonics like the Hercynian orogeny or the Tethyan opening [*Sanchez-Rodriguez and Gebauer*, 2000], but they also documented ages between 25 and 22 Ma that fall within the time range of the Betic-Rif orogeny.

[26] The peridotite emplacement has been qualified as a hot emplacement based on the occurrence of a dynamothermal aureole underlying the peridotite [*Westerhof*, 1977; *Lundeen*, 1978; *Tubía et al*., 1997; *Esteban et al*., 2008]. This feature suggests a high temperature of the basal peridotite during its emplacement, in favor of the early Miocene timing for the peridotite deformation. Indeed, a deformation occurring during Paleozoic-Mesozoic time would imply that the peridotite remained at midcrustal depth for several tens of million years before to be emplaced onto the crust and, hence, that its thermal state would be entirely equilibrated at the time of the emplacement. In contrast, if the deformation of the peridotite occurred between 25 and 22 Ma, i.e., just before the emplacement at 22 Ma, the thermal state of the peridotite would have been highly in disequilibrium during the emplacement. However, we cannot stress on this hypothesis because we have no constraint on the peridotite temperature required to form the dynamothermal aureole, i.e., to produce syn-emplacement partial melting of the overlapped crust.

[27] A thorough data set has been provided in the last 40 years concerning the geometry and the *P-T* path of the dynamothermal aureole beneath the Ronda peridotite [*Esteban et al*., 2008, and references therein]. It has been shown that thrusting of the peridotite promoted partial melting of the Blanca unit over a thickness between 100 and 200 m. *Esteban et al*. [2008] also documented the aureole *P-T* path that indicates 4 kbar/540°C before partial melting of the metapelitic rocks and 6 kbar/750°C during partial melting and mylonitization (Figure 10a). The *P-T* path finally documents a subsequent decompression of the aureole related to the post-emplacement history of the Blanca unit. We will discuss this latter point in section 6. Regardless of tectonic overpressure, such a *P-T* path suggests therefore that the thinned lithosphere section, including the peridotite, was around 18 km thick (6 kbar) during overlapping of the aureole protolith at 12 km depth (4 kbar). On these bases, we propose to quantify the peridotite temperature at the base of the lithosphere section required to promote partial melting of the Betic crust (Blanca unit) over a thickness of 100–200 m during the peridotite emplacement.

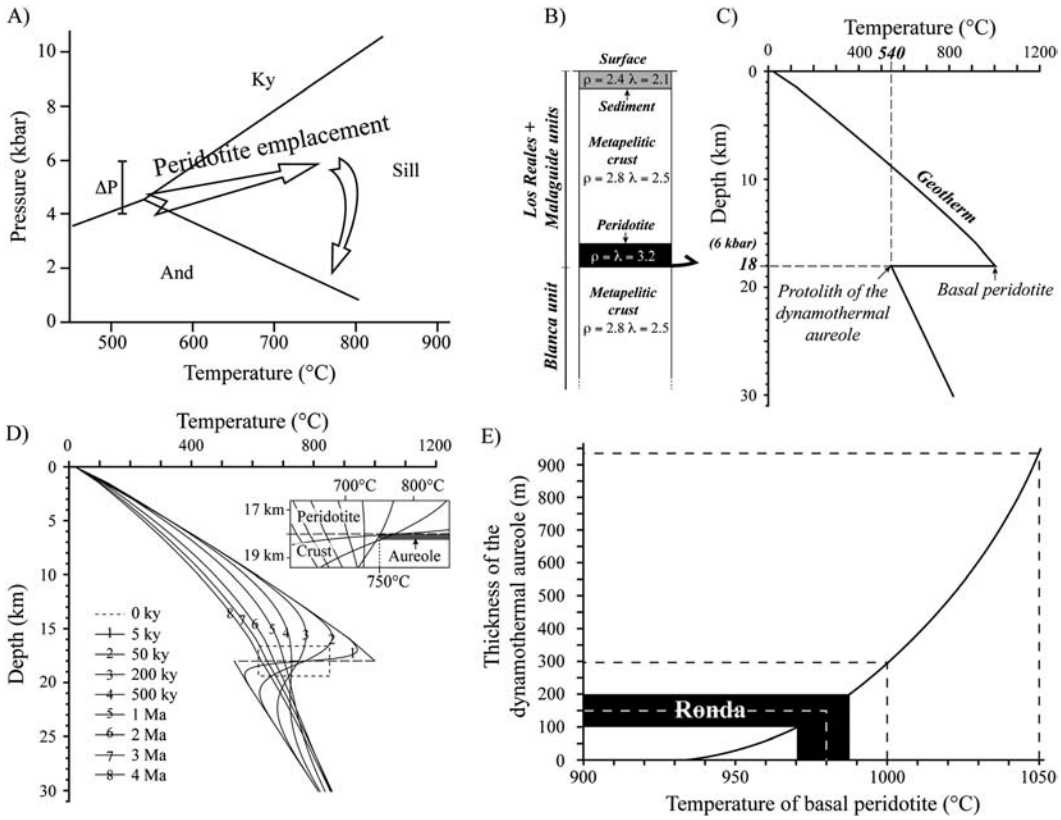

Figure 10. (a) Pressure-temperature path of the dynamothermal aureole (modified after *Esteban et al.* [2008]): And = Andalousite; Ky = Kyanite; Sill = Sillimanite. (b) Input of the numerical model that accounts for the upper Blanca unit [radiogenic metapelitic rocks: density (ρ) = 2800 kg m^{-3}; thermal diffusivity (λ) = 2.5] and the Los Reales unit, including 2 km of peridotite (ρ = 3200 kg m^{-3}; λ = 3.2), 14.5 km of radiogenic metapelitic crust (ρ = 2800 kg.m^{-3}; λ = 2.5), and 1.5 km of sediment (ρ = 2400 kg m^{-3}; λ = 2.1). Layer thicknesses and rocks properties are from *Tubía et al.* [1992] and *Soto et al.* [2008], respectively. (c) Geotherm of the model before thermal balance. Based on the *P-T* data set from *Esteban et al.* [2008], the tectonic contact between the peridotite and the Blanca unit has been set at 18 km depth (6 kbar) with a temperature of 540°C for the top Blanca unit (protolith of the dynamothermal aureole) and a higher temperature for the basal peridotite. (d) Example of thermal balance over 4 million years with a starting temperature of 1000°C at the base of the peridotite. In this case, we expect around 300 m of aureole thickness (peridotite-underlying rocks above 750°C). (e) Thickness of the dynamothermal aureole (*Y* axis) with respect to the initial temperature of the basal peridotite (*X* axis). Because the thickness of the aureole in Ronda ranges between 100 and 200 m, this graph indicates a basal peridotite temperature between 970°C and 988°C at the time of the peridotite emplacement (see text).

5.1. Numerical Setting

[28] We implemented a one-dimensional implicit finite difference model that solved the heat equation for a metapelitic crustal section of 30 km thick [*Gueydan et al.*, 2009], including 1.5 km of top sediment and 2 km of mantle peridotite above 18 km depth, such as indicated by the syn-emplacement pressure of the aureole *P-T* path (6 kbar, Figure 10b). We used the following form of the heat equation:

$$k.\frac{\partial T}{\partial t} = \rho \cdot C_p \cdot \frac{\partial^2 T}{\partial x^2} + r$$

where T is the temperature, t is the time, x is the depth, ρ is the density, C_p is the thermal capacity, k is the thermal conductivity, and r is the term for radioactivity. We assumed an exponential decrease of the radioactivity with depth based on the following equation [*Burov and Watts*, 2006]:

$$r(x) = r_0 \cdot \exp\left(-\frac{x}{H}\right)$$

where r_0 is a constant, and H is the total thickness of the crustal section. All thermal and mechanical constants are from *Burov and Watts* [2006] and *Soto et al.* [2008] and are given in Table 1. Starting conditions have been set up at the time of the hot emplacement before the thermal balance between the hanging wall and the footwall of the emplacement fault at 18 km depth (Figure 10c). The initial geotherm has been also set up such that the top temperature of the footwall is at 540°C and the bottom temperature of the hanging wall is at a higher temperature (Figure 10c). The surface temperature is 20°C. We then calculated the thermal balance over a time of 4 Ma and tested several initial geotherms of the

Table 1. Values and Constants Used in the Numerical Model[a]

Constant	Value
Sediment density (ρ_s)[b] (kg m^{-3})	2400
Crust density (ρ_c)[b] (kg m^{-3})	2800
Mantle density (ρ_m)[b] (kg m^{-3})	3200
Sediment thermal conductivity (k_s)[b] (W m^{-1} K^{-1})	2.1
Crust thermal conductivity (k_c)[b] (W m^{-1} K^{-1})	2.5
Mantle thermal conductivity (k_m)[b] (W m^{-1} K^{-1})	3.2
Specific thermal capacity (C_p) (J kg^{-1} K^{-1})	1000
Surface heat production (r_0) [c](W m^{-3})	2.56
Thickness of the crustal section (H) [d] (km)	30
Thickness of sediment[d] (km)	1.5
Thickness of peridotite [d] (km)	2
Surface temperature (°C)	20

[a]Thermal and mechanical constants after *Soto et al*. [2008], surface heat production after *Burov and Watts* [2006], and thicknesses after *Tubía et al*. [1992].
[b]*Soto et al*. [2008].
[c]*Burov and Watts* [2006].
[d]*Tubía et al*. [1992].

hanging wall using the basal temperature of peridotite as the major unknown.

5.2. Results

[29] In Figure 10d, we show an example of a thermal balance for a basal peridotite temperature of 1000°C. Such a balance promotes (1) rapid cooling of 200°C/Ma to 400°C/Ma for the peridotite and (2) a fast increase in temperature for the first top meters of the Blanca unit, reaching more than 750°C below the peridotite, i.e., the partial melting point of the metapelitic Blanca rocks. The rapid cooling of peridotite occurs in the first million years, and then, the cooling rate decreases from 40°C/Ma to 50°C/Ma during the second million years to less than 20°C/Ma to 30°C/Ma after 3 Ma of thermal balance. Concerning the top Blanca unit, partial melting occurs within the first one hundred thousand years of thermal balance. Then, the heat is progressively transferred downward, promoting a moderate increase in temperature at the base of the section and a temperature drop in the uppermost layer beneath the peridotite. Similarly to the peridotite, the temperature drops rapidly in the first million years (~100°C/Ma to 150°C/Ma), and then, the cooling rate decreases progressively down to less than 10°C/Ma 20°C/Ma after 3 Ma of thermal balance.

[30] On these bases and in order to constrain the minimum basal peridotite temperature required to form the dynamothermal aureole, we calculated the thickness of the partially melted layer ($T > 750$°C) for a basal peridotite temperature ranging from 900°C to 1050°C (Figure 10e). For temperature below 930°C, the emplacement of the Ronda peridotite does not involve any partial melting of the overlapped crust. Above 930°C, the thickness of the partially melted layer increases exponentially with increasing temperature. We expect, for example, an aureole thickness of around 300 m for a basal temperature of 1000°C and 930 m for a temperature of 1050°C, respectively. The thickness of the dynamothermal aureole observed below the Ronda peridotite ranges between 100 and 200 m. Our numerical results thus suggest a syn-emplacement basal temperature of the peridotite between 970°C and 988°C, with a mean temperature at 980°C (Figure 10e).

[31] A temperature of 980°C at 18 km depth documents here a highly transient thermal gradient for a continental lithosphere at the time of the peridotite emplacement. Such a thermal gradient is very unlikely for peridotite lying at midcrustal depth for several million years. In contrast, it strongly suggests that the southern Ronda peridotite was still hot and therefore deforming just before its crustal emplacement. The ductile deformation of the Ronda peridotite (e.g., kilometer-scale mantle shear zone, partial melting, and subsequent plagioclase deformation) therefore occurs most probably during the late Oligocene–early Miocene, probably between 30 and 22 Ma, just before the emplacement time at 22 Ma.

6. Deformation and Exhumation of the Ronda Peridotite

6.1. Geodynamic Context

[32] In previous studies, the deformation and exhumation of the Ronda peridotite has been first attributed to mylonitization along a subduction slab and then an uplift due to the occurrence of lithosphere-scale detachments during slab break off and gravitational collapse of the Betic-Rif chain [*Tubía et al*., 1992; *Van der Wal and Vissers*, 1993; *Platt et al*., 2003b]. *Van der Wal and Vissers* [1993] based their interpretation on the hypotheses of (1) diachronous and uncorrelated deformation between the Grt/Spl mylonite and the Spl tectonite and (2) pressure increase during mylonitization. However, *Garrido et al*. [2011] and our results, respectively, show that both the Grt/Spl mylonite and the Spl tectonite suffered a unique decompression and synchronous penetrative stretching coeval with ductile strain localization. Our observations suggest therefore that the Ronda mantle shear zone originates from a tectonic context involving syn-uplift mylonitization of the peridotite. The occurrence of syn-tectonic partial melting in the granular domain confirms this hypothesis.

[33] *Platt et al*. [2003b] then proposed the successive occurrence of three extensional detachments during slab break off and gravitational collapse of the Betic-Rif orogen to account for thermobarometric and chronological data in the peridotite and its crustal envelope. The emplacement of the peridotite was attributed to the second detachment, following the interpretation of *Tubía et al*. [1992]. However, detailed studies on the dynamothermal aureole beneath the peridotite showed that pressure increased during the peridotite emplacement (Figure 10a) [*Esteban et al*., 2008] and, hence, that mantle rocks overlapped the crust during a thrusting event and not along an extensional detachment [*Westerhof*, 1977; *Lundeen*, 1978; *Tubía and Cuevas*, 1987; *Esteban et al*., 2008].

[34] A recent model of mantle extrusion along a subducting slab in a context of transpressive deformation has been also proposed to explain the exhumation of the Ronda peridotite [*Mazzoli and Algarra*, 2011; *Tubía et al*., 2012]. However, this model does not account for (1) the structural thinning of the Jubrique unit [*Balanyá et al*., 1997; *Argles et al*., 1999; *Sanchez-Gomez et al*., 2002], (2) the structural consistency between the Ronda shear zone and the overlying Jubrique unit [*Balanyá et al*., 1997], and (3) the syn-deformation uplift of the lithosphere-asthenosphere boundary [*Soustelle et al*., 2009; this study].

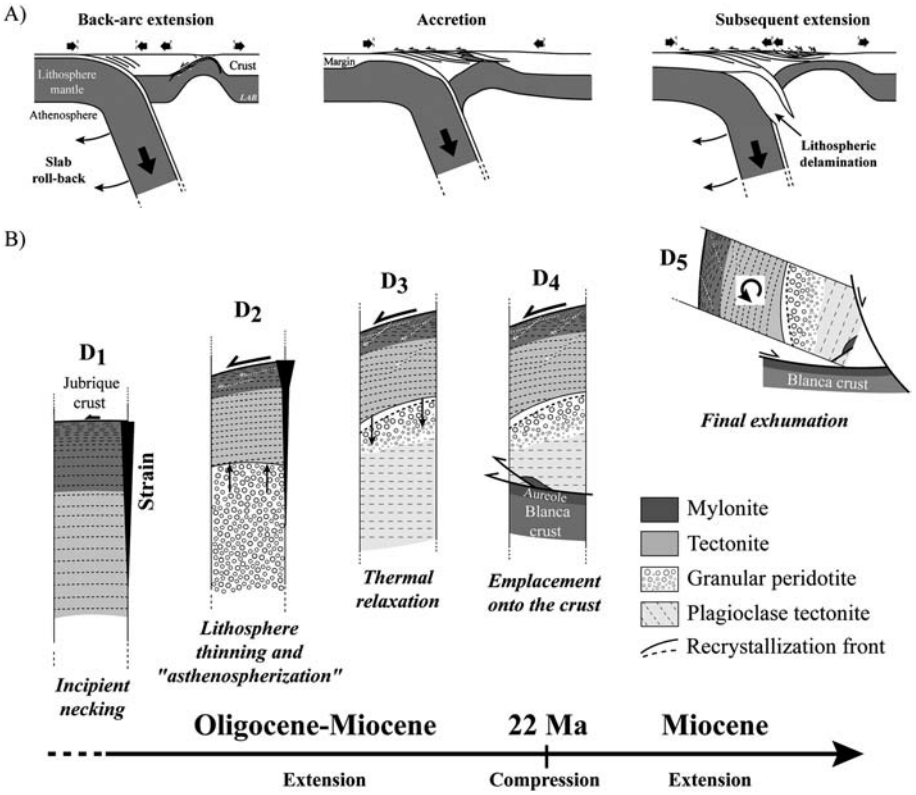

Figure 11. (a) Sketches illustrating the uplift and exhumation of the Ronda peridotite during subduction slab rollback (modified after *Booth-Rea et al*. [2005]). In this context, we hypothesize that mantle rocks were uplifted beneath a back-arc extension and then accreted onto a subducting margin during inversion of the back-arc rift and finally exhumed during extension induced by subsequent lithospheric delamination. (b) Schematic logs illustrating the internal deformation of the Ronda peridotite during uplift and exhumation. (D1) Incipient viscous strain localization in the uppermost mantle, triggering necking of the continental lithosphere. (D2) Development of the Spl tectonite, the Grt/Spl mylonite, and the S-C–type structures induced by further strain localization; coeval uplift of the lithosphere-asthenosphere boundary (granular peridotite) during lithosphere thinning/rifting. (D3) Development of high-angle shear bands induced by further continental necking and steepening of the main shear plane; isolation of the granular peridotite and formation of the plagioclase tectonite due to syn-thinning thermal relaxation. (D4) Emplacement/accretion of the Ronda peridotite onto the crust (Blanca unit) and formation of the dynamothermal aureole during inversion of the back-arc rift 22 Ma ago. (D5) Final exhumation and tilting of the Ronda massif resulting from the Miocene extension that we attribute to subsequent lithospheric delamination [*Duggen et al*., 2008].

[35] Finally, *Booth-Rea et al*. [2005] and *Garrido et al*. [2011] proposed that the exhumation of the Ronda peridotite resulted from the inversion of a back-arc continental rift in a context of slab rollback during the Oligocene-Miocene [*Royden*, 1993; *Lonergan and White*, 1997, *Rosenbaum et al*., 2002; *Lacombe and Jolivet*, 2005]; they relate the back-arc rift inversion to the subduction of the Iberian passive margin. In such a slab rollback-related model, the following geodynamical events are expected: (1) extensive back-arc thinning of the continental crust, (2) an uplift of the lithosphere mantle at a very shallow depth, and, then, (3) an accretion of a thinned lithosphere onto the subducting plate. This model, moreover, involves 4) a delamination of the lithospheric mantle that follows the accretion [*Duggen et al*., 2008], giving rise to a continuous alternation of extensional and compressional stages in a short period of time (Figure 11a). In this paper, we show available data and document features of both the Ronda peridotite and its crustal envelope whose the slab rollback model may account for. This includes (1) extensive structural thinning of the peridotite-overlying crustal section (Jubrique unit), (2) a syn-tectonic decompression of the Ronda peridotite up to midcrustal depth, (3) an emplacement/accretion of the peridotite and its crustal envelope that follows the uplift, and (4) a subsequent extension that terminates the exhumation. All these events occurred during the Oligocene-Miocene in a short period of time (less than 20 Ma). We thus propose in the following sections to account for the deformation and exhumation of the Ronda peridotite in a context of subduction slab rollback.

6.2. Mantle Uplift During Lithosphere Thinning

[36] The Ronda mantle shear zone represents the oldest structural domain preserved in the Ronda peridotite. We propose that such a deformation originates from strain localization during back-arc continental extension and lithosphere thinning/necking, in which we involve progressive transition from near coaxial thinning (Figure 11b, D_1) to noncoaxial deformation within a mantle shear zone (Figure 11b, D_2).

Strain localization occurred in the Ronda mylonite as a result of grain size reduction and subsequent activation of low-temperature grain size–sensitive processes [*Précigout et al*., 2007; *Précigout and Gueydan*, 2009]. We thus propose that lithosphere necking originates here from the occurrence of low-temperature subcrustal strain localization, which implies the combination of coaxial and noncoaxial deformation components in different amounts. While coaxial deformation dominates at incipient extension, the shear deformation component becomes more and more dominant as continental necking takes place. We relate the development of S-C structures to this deformation stage. We then attribute the development of discrete shear bands at ~40° of the shear zone to the subsequent steepening of the main shear plane induced by further continental thinning (Figure 11b, D_3).

6.3. Syn-thinning Asthenospherization

[37] Coevally, the base of the shear zone protolith (Spl tectonite) has been affected by asthenosphere-related partial melting, forming the so-called granular peridotite. Following *Van der Wal and Vissers* [1996] and *Lenoir et al*. [2001], we attribute this event to an uplift of the thermally controlled lithosphere-asthenosphere boundary (LAB; recrystallization front) through the basal lithosphere (Spl tectonite). However, we propose that such an uplift of the LAB occurred during necking and shear zone–induced thinning of the continental lithosphere (Figure 11b, D_2). Indeed, the occurrence of deep partial melting is commonly described during continental lithosphere thinning, as well as the development of an overlying large-scale shear zone preserving high-pressure/low-temperature rocks along a near-adiabatic decompressive *P-T* path. We therefore relate the partial melting of the Ronda peridotite to the dynamics of continental extension. In this context, while strain localization occurs in the uppermost mantle, "asthenospherization" promotes grain coarsening of the basal lithosphere without affecting the geometry of strain-induced structures (pyroxenite folds, LPO). Syn-thinning partial melting of the basal lithosphere also accounts for the intrusion and subsequent folding of pyroxenite dykes (Cr-rich pyroxenite) within the overlying shear zone (Figure 8).

6.4. Syn-thinning Thermal Relaxation

[38] Following the partial melting of the southern Ronda massif, the base of the partially molten granular peridotite was subsequently affected by a new penetrative foliation and subsolidus plagioclase, forming the plagioclase tectonite domain. This event implies a drop in temperature from the melting point of the peridotite, which occurred prior to the peridotite emplacement [*Van der Wal and Vissers*, 1996]. To account for this feature, we propose rapid cooling from the top section (mantle shear zone) downward, i.e., a thermal relaxation of the basal lithosphere (Figure 11b, D_3). We attribute this downward cooling to the uplift of the mantle section along the mantle shear zone that gets mantle rocks closer to the colder, shallower crust. Such a phenomenon accounts for (1) a drop in temperature in the granular domain, fast enough to preserve coarse-grained peridotite and pristine spinel despite rift-induced decompression; and (2) slower cooling in deeper peridotite that permitted promoting new thinning-induced deformation and appearance of syn-kinematic plagioclase upon decompression. Note that the downward cooling of the Ronda mantle section is required to preserve an undeformed and plagioclase-free domain (granular peridotite) beneath the Spl tectonite.

6.5. Emplacement and Exhumation

[39] We then propose that the emplacement of the peridotite occurred due to a major thrust during inversion of this continental thinning (Figure 11b, D_4). At the time of the peridotite emplacement (≈22 Ma) [*Esteban et al*., 2011], the base of the Ronda peridotite was around 980°C at 18 km depth, as required to form the dynamothermal aureole (Figure 10). This result indicates that the thermal state of the lithosphere section, including the peridotite, was extremely transient and, hence, that thermal relaxation was probably occurring during the inversion of the continental rift and the emplacement of the peridotite. Such a feature suggests that the peridotite emplacement occurred just after its decompression during lithosphere thinning (Figure11b, D_4). In this context, the emplacement promoted intense cooling of the Ronda peridotite, which then acted as a rigid body within the Alpujarride crust. Such cooling is recorded in both the Blanca and Los Reales units from 21 Ma onward [*Esteban et al*., 2004].

[40] Finally, the internal Betics experienced brittle normal faulting and bloc tilting owing to extensional setting during the Miocene, which probably led to the opening of the Alboran basin [*Rossetti et al*., 2005, and references therein]. Some authors attribute this extensional event to the delamination of the lithosphere mantle following the subduction of the Iberian passive margin [*Duggen et al*., 2008]. This context has promoted tectonic exhumation—associated with erosion—of the peridotite-underlying Blanca unit [*Garcia-Dueñas et al*., 1992; *Sanchez-Gomez et al*., 2002]. We therefore suggest that the final exhumation of the Ronda peridotite results from the Miocene extension of the internal Betics following its emplacement. This event promoted northwestward tilting of the lithosphere section, including both the peridotite and the overlying Jubrique unit (Figure 11b, D_5).

7. Conclusion

[41] We compile in this paper available data and document structural features in the western Ronda peridotite that both describe three successive stages of deformation. First, there is the formation of a large-scale mantle shear zone (Grt/Spl mylonite and Spl tectonite) resulting from strain localization during intense thinning of the continental lithosphere (Jubrique crust and Ronda peridotite) with syn-thinning partial melting of the basal shear zone protolith (granular peridotite). The deformation regime of this shear zone evolved from penetrative stretching to discrete sinistral shear. Both strain localization and partial melting occurred during decompression from more than 18 kbar/60 km to less than 10 kbar/30 km. Second, a viscous deformation of the basal Ronda peridotite prior to its emplacement yields to the formation of a new plagioclase-bearing foliation during decompression from more than 10 kbar/30 km to around 6 kbar/18 km. These two deformation events occurred during strong continental lithosphere thinning. Finally, a third deformation involved thrusting at 22 Ma of a strongly thinned continental lithosphere on top of the crustal rocks, which were coevally

partially melted (Blanca unit). Our numerical thermal models show that continental lithosphere thinning (crust and mantle) should have occurred just before thrusting of the peridotite at 22 Ma, probably between 30 and 22 Ma, in order to promote partial melting of the overlapped crust.

[42] We propose that the deformation and exhumation of the Ronda peridotite results from continental extension and subsequent thrusting during the Oligocene-Miocene. The dynamics of westward slab rollback through the Alboran region supplies a consistent model to account for this process of exhumation. However, we stress that additional investigations are required to demonstrate the relationships between slab rollback and exhumation of subcontinental mantle. We nonetheless put forward the thrusting of a back-arc thinned continental lithosphere as a possible process of exhumation for subcontinental mantle, which should be considered in future studies.

References

Afiri, A., F. Gueydan, P. Pitra, A. Essaifi, and J. Précigout (2011), Oligo-Miocene exhumation of the Beni-Bousera peridotite through a lithosphere-scale extensional shear zone, *Geodin. Acta*, *24*(1), 49–60.

Andrieux, J., J. M. Fontboté, and M. Mattauer (1971), Sur un modèle explicatif de l'arc de Gibraltar, *Bull. Soc. Geol. Fr.*, *15*, 555–569.

Argles, T. W., J. P. Platt, and D. J. Waters (1999), Attenuation and excision of a crustal section during extensional exhumation: The Carratraca massif, Betic Cordillera, southern Spain, *J. Geol. Soc. London*, *156*, 149–162.

Augier, R., P. Agard, P. Monié, L. Jolivet, C. Robin, and G. Booth-Rea (2005), Exhumation, doming and slab retreat in the Betic Cordillera (SE Spain): In situ $^{40}Ar/^{39}Ar$ ages and *P-T-d-t* paths for the Nevado-Filábride complex, *J. Metamorph. Geol.*, *23*, 357–381.

Azañon, J. M., and A. Crespo-Blanc (2000), Exhumation during a continental collision inferred from the tectonometamorphic evolution of the Alpujarride Complex in the central Betics (Alboran Domain, SE Spain), *Tectonics*, *19*, 549–565.

Azañon, J., and B. Goffé (2005), Ferro- and magnesiocarpholite assemblages as record high-P, low-T metamorphism in the Central Alpujarrides, Betic Cordillera (SE Spain), *Eur. J. Mineral.*, *9*, 1035–1051.

Balanyá, J. C., and V. Garcia-Dueñas (1987), Structural trends of the Alboran Domain on both sides of the straits of Gibraltar, *C. R. Acad. Sci.*, *334*(15), 929–932.

Balanyá, J. C., V. Garcia-Dueñas, J. M. Azañon, and M. Sánchez-Gómez (1997), Alternating contractional and extensional events in the Alpujarride nappes of the Alboran Domain, *Tectonics*, *16*, 226–238.

Berthé, D., P. Choukroune, and P. Jegouzo (1979), Orthogneiss, mylonite, and non coaxial deformation of granites: The example of the South American Shear Zone, *J. Struct. Geol.*, *1*(1), 31–42.

Blichert-Toft, J., F. Albarède, and J. Kornprobst (1999), Lu-Hf isotope systematics of garnet pyroxenites from Beni Bousera, Morocco: Implications for basalt origin, *Science*, *283*, 1303–1306.

Bodinier, J. L., C. J. Garrido, I. Chanefo, O. Bruguier, and F. Gervilla (2008), Origin of pyroxenite-peridotite veined mantle by refertilization reactions: Evidence from the Ronda peridotite (southern Spain), *J. Petrol.*, *49*(5), 999–1025.

Booth-Rea, G., J. M. Azañon, J. M. Martinez-Martinez, O. Vidal, and V. Garcia-Dueñas (2005), Contrasting structural and *P-T* evolution of tectonic units in the southeastern Betics: Key for understanding the exhumation of the Alboran Domain HP/LT crustal rocks (western Mediterranean), *Tectonics*, *24*, TC2009, doi:10.1029/2004TC001640.

Burov, E. B., and A. B. Watts (2006), The long-term strength of continental lithosphere: "Jelly sandwich" or "crème brûlée"?, *GSA Today*, *16*, 4–10.

Cuevas, J., J. J. Esteban, and J. M. Tubía (2006), Tectonic implications of the granite dyke swarm in the Ronda peridotites (Betic Cordilleras, southern Spain), *J. Geol. Soc.*, *163*, 631–640.

Davies, G. R., P. H. Nixon, D. G. Pearson, and M. Obata (1993), Tectonic implications of graphitized diamonds from the Ronda peridotite massif, southern Spain, *Geology*, *21*, 471–474.

Doblas, M., and R. Oyarzun (1989), Mantle core complexes and Neogene extensional detachment tectonics in the western Betic Cordilleras, Spain: An alternative model for the emplacement of the Ronda peridotite, *Earth Planet. Sci. Lett.*, *93*, 76–84.

Duggen, S., K. Hoernle, A. Klügel, J. Geldmacher, M. Thirlwall, F. Hauff, D. Lowry, and N. Oates (2008), Geochemical zonation of the Miocene Alboran Basin volcanism (westernmost Mediterranean): Geodynamic implications, *Contrib. Mineral. Petrol.*, *156*, 577–593.

Esteban, J. J., L. Sanchez-Rodriguez, D. Seward, J. Cuevas, and J. M. Tubía (2004), The late thermal history of the Ronda area, southern Spain, *Tectonophysics*, *389*, 81–92.

Esteban, J. J., J. Cuevas, N. Vegas, and J. M. Tubía (2008), Deformation and kinematics in a melt-bearing shear zone from the western Betic Cordilleras (southern Spain), *J. Struct. Geol.*, *30*, 380–393.

Esteban, J. J., J. Cuevas, J. M. Tubía, S. Sergeev, and A. Larionov (2011), A revised Aquitanian age for the emplacement of the Ronda peridotites (Betic Cordilleras, southern Spain), *Geol. Mag.*, *148*(1), 183–187.

Garcia-Dueñas, V., J. C. Balanyá, and J. M. Martinez-Martinez (1992), Miocene extensional detachments in the outcropping basement of the northern Alboran Basin (Betics) and their tectonic implications, *Geo Mar. Lett.*, *12*, 88–95.

Garrido, C. J., and J. L. Bodinier (1999), Diversity of mafic rocks in the Ronda peridotite: Evidence for pervasive melt-rock reaction during heating of subcontinental lithosphere by upwelling asthenosphere, *J. Petrol.*, *40*, 729–754.

Garrido, C. J., F. Gueydan, G. Booth-Rea, J. A. J. Précigout, K. Hydas, J. A. Padron-Navarta, and C. Marchesi (2011), Garnet lherzolite and garnet-spinel mylonite in the Ronda peridotite: Vestiges of Oligocene backarc mantle lithospheric extension in the western Mediterranean, *Geology*, *39*(10), 927–930, doi:10.1130/G31760.1.

Gueydan, F., E. Le Garzic, and N. Carry (2009), P/T ratio in high-pressure rocks as a function of dip and velocity of continental subduction, *Lithosphere*, *1*, 282–290.

Hidas, K., G. Booth-Rea, C. J. Garrido, J. M. Martínez-martínez, J. A. Padrón-Navarta, Z. Konc, F. Giaconia, E. Frets, and C. Marchesi (2013), Backarc basin inversion and subcontinental mantle emplacement in the crust: kilometer-scale folding and shearing at the base of the proto-Alboran lithospheric mantle (Betic Cordillera, southern Spain), *J. Geol. Soc. London*, *170*, 47–55, doi:10.1144/jgs2011-151.

Lacombe, O., and L. Jolivet (2005), Structural and kinematic relationships between Corsica and the Pyrenees-Provence domain at the time of the Pyrenean orogeny, *Tectonics*, *24*, TC1003, doi:10.1029/2004TC001673.

Lenoir, X., C. J. Garrido, J. L. Bodinier, J. M. Dautria, and F. Gervilla (2001), The recrystallization front of the Ronda peridotite: Evidence for melting an thermal erosion of subcontinental lithospheric mantle beneath the Alboran Basin, *J. Petrol.*, *42*, 141–158.

Lonergan, L. (1993), Timing and kinematics of deformation in the Malaguide complex, internal zone of the Betic Cordillera, Southeast Spain, *Tectonics*, *12*, 460–476.

Lonergan, L., and N. White (1997), Origin of the Betic-Rif mountain belt, *Tectonics*, *16*, 504–522.

Loomis, T. P. (1975), Tertiary mantle diapirism, orogeny and plate tectonics east of the strain of Gibraltar, *Am. J. Sci.*, *275*, 1–30.

Luján, M., J. C. Balanyá, and A. Crespo-Blanc (2000), Contractional and extensional tectonics in flysch and penibetic units (Gibraltar Arc, SW Spain): New constraints on emplacement mechanisms, *Earth Planet. Sci.*, *330*, 631–638.

Luján, M., A. Crespo-Blanc, and J. C. Balanyá (2006), The Flysch Trough thrust imbricate (Betic Cordillera): A key element of the Gibraltar Arc orogenic wedge, *Tectonics*, *25*, TC6001, doi:10.1029/2005TC001910.

Lundeen, M. T. (1978), Emplacement of the Ronda peridotite, Sierra Bermeja, Spain, *Geol. Soc. Am. Bull.*, *89*, 172–180.

Mazzoli, S., and A. M. Algarra (2011), Deformation partitioning during transpressional of a "mantle extrusion wedge": The Ronda peridotites, western Betic cordillera, Spain, *J. Geol. Soc. London*, *168*, 373–382, doi:10.1144/0016-76492010-126.

Monié, P., R. L. Torres-Roldan, and A. García-Casco (1994), Cooling and exhumation of the western Betic Cordilleras, $^{40}Ar/^{39}Ar$ thermochronological constraints on a collapse terrane, *Tectonophysics*, *238*, 353–379.

Morishita, T., S. Arai, and F. Gervilla (2001), High-pressure aluminous mafic rocks from the Ronda peridotite massif, southern Spain: Significance of sapphirine- an corundum-bearing mineral assemblages, *Lithos*, *57*, 143–161.

Negro, F., O. Beyssac, B. Goffé, O. Saddiqi, and M. L. Bouybaouene (2006), Thermal structure of the Alboran Domain in the Rif (northern Morocco) and the western Betics (southern Spain). Constraints from Raman spectroscopy of carbonaceous material, *J. Metamorph. Geol.*, *24*, 309–327.

Obata, M. (1980), The Ronda peridotite: Garnet-, spinel-, and plagioclase-lherzolite facies and the *P-T* trajectories of a high-temperature mantle intrusion, *J. Petrol.*, *21*, 533–572.

Obata, M. (1994), Material transfer and local equilibria in a zoned kelyphite from a garnet pyroxenite, Ronda, Spain, *J. Petrol.*, *35*, 271–287.

Pearson, D., G. R. Davies, and P. H. Nixon (1995), Orogenic ultramafic rocks of UHP (diamond facies) origin, in *Utrahigh Pressure Metamorphism*, edited by R. G. Coleman, and X. Wang, pp. 456–511, Cambridge Univ. Press, New York.

Platt, J. P., S. Allerton, A. Kirker, C. Mandeville, A. Mayfield, E. S. Platzman, and A. Rimi (2003a), The ultimate arc: Differential displacement, oroclinal bending, and vertical axis rotation in the external Betic-Rif arc, *Tectonics*, *22*, TC1017, doi:10.1029/2001TC001321.

Platt, J. P., T. W. Argles, A. Carter, S. P. Kelley, M. J. Whitehouse, and L. Lonergan (2003b), Exhumation of the Ronda peridotite and its crustal envelope: Constraints from thermal modelling of a *P-T*-time array, *Q. J. Geol. Soc. London*, *160*, 655–676.

Platt, J. P., S. P. Kelley, A. Carter, and M. Orozco (2005), Timing of tectonic events in the Alpujárride Complex, Betic Cordillera, southern Spain, *Q. J. Geol. Soc. London*, *162*, 1–12.

Platt, J. P., R. Anczkiewicz, J.-I. Soto, S. P. Kelley, and M. Thirlwall (2006), Early Miocene continental subduction and rapid exhumation in the western Mediterranean, *Geology*, *34*(11), 981–984, doi:10.1130/G22801A.1.

Précigout, J., and F. Gueydan (2009), Mantle weakening and strain localization: Implications for the long-term strength of the continental lithosphere, *Geology*, *37*(2), 147–150.

Précigout, J., F. Gueydan, D. Gapais, C. J. Garrido, and A. Essaifi (2007), Strain localisation in the sub-continental mantle—A ductile alternative to the brittle mantle, *Tectonophysics*, *445*, 318–336.

Priem, J. P., N. A. I. M. Boelrijk, E. H. Hebeda, I. S. Oen, E. A. T. Verdurmen, and R. H. Verschure (1979), Isotopic dating of the emplacement of the ultramafic masses in the Serrania de Ronda, southern Spain, *Contrib. Mineral. Petrol.*, *70*, 103–109.

Puga, E., J. M. Diaz de Federico, J.-L. Bodinier, and L. Morten (1999), Petrology and metamorphic evolution of ultramafic rocks and dolerite dykes of the Betic Ophiolite Association (Mulhacen Complex, SE Spain): Evidence of eo-Alpine subduction following an ocean-floor metasomatic process, *Lithos*, *49*, 23–56.

Ramsay, J. G. (1982), Rock ductility and its influence on the development of tectonic structures in mountain belts, in *Mountain Building Processes*, edited by K. J., Hsü, pp. 111–127, Academic, London.

Rosenbaum, G., G. S. Lister, and C. Duboz (2002), Reconstruction of the tectonic evolution of the western Mediterranean since the Oligocene, *J. Virtual Explor.*, *8*, 107–130.

Rossetti, F., C. Faccenna, and A. Crespo-Blanc (2005), Structural and kinematic constraints to the exhumation of the Alpujarride complex (central Betic Cordillera, Spain), *J. Struct. Geol.*, *27*, 199–216.

Royden, L. H. (1993), Evolution of retreating subduction boundaries formed during continental collision, *Tectonics*, *12*, 629–638.

Sanchez-Gomez, M., J. C. Balanyá, V. Garcia-Dueñas, and J. M. Azañon (2002), Intracrustal tectonic evolution of large lithosphere mantle slabs in the western end of the Mediterranean orogen (Gibraltar arc), *J. Virtual Explor.*, *8*, 23–34.

Sanchez-Rodriguez, L., and D. Gebauer (2000), Mesozoic formation of pyroxenites and gabbros in the Ronda area (southern Spain), followed by early Miocene subduction metamorphism and emplacement into the middle crust: U-Pb sensitive high-resolution ion microprobe dating of zircon, *Tectonophysics*, *316*, 19–44.

Soto, J. I., F. Fernández-Ibáñez, M. Fernández, and A. García-Casco (2008), Thermal structure of the crust in the Gibraltar Arc: Influence on active tectonics in the western Mediterranean, *Geochem. Geophys. Geosyst.*, *9*, Q10011, doi:10.1029/2008GC002061.

Soustelle, V., A. Tommasi, J.-L. Bodinier, C. J. Garrido, and A. Vauchez (2009), Deformation and reactive melt transport in the mantle lithosphere above a large-scale partial melting domain: The Ronda peridotite massif, southern Spain, *J. Petrol.*, *50*(7), 1235–1266.

Torné, M., E. Banda, V. García Dueñas, and J. C. Balanyá (1992), Mantle-Lithosphere bodies in the Alboran crustal domain (Ronda peridotites, Betic-Rif orogenic belt), *Earth Planet. Sci. Lett.*, *110*, 163–171.

Tubía, J. M., and J. Cuevas (1987), Structures et cinematique liées a la mise en place des péridotites de Ronda (Cordillères Bétiques, Espagne), Geodin. Acta, *1*(1), 59–69.

Tubía, J. M., J. Cuevas, F. Navarro Vila, F. Alvarez, and F. Aldaya (1992), Tectonic evolution of the Alpujarride Complex (Betic Cordillera, southern Spain), *J. Struct. Geol.*, *14*, 193–203.

Tubía, J. M., F. Navarro-Vilá, and J. Cuevas (1993), The Maláguide-Los Reales Nappe: An example of crustal thinning related to the emplacement of the Ronda peridotites (Betic Cordillera), *Phys. Earth Planet. Inter.*, *78*, 343–354.

Tubía, J. M., J. Cuevas, and J. I. Gil Ibarguchi (1997), Sequential development of the metamorphic aureole beneath the Ronda peridotites and its bearing of the tectonic evolution of the Betic Cordillera, *Tectonophysics*, *279*, 227–252.

Tubía, J. M., J. Cuevas, and J. J. Esteban (2004), Tectonic evidence in the Ronda peridotites, Spain, for mantle diapirism related to delamination, *Geology*, *32*, 941–944.

Tubía, J. M., J. Cuevas, and J. J. Esteban (2012), Localization of deformation and kinematic shift during the hot emplacement of the Ronda peridotites (Betic Cordilleras, southern Spain), *J. Struct. Geol.*, *50*, 148–160.

Van der Wal, D., and J. L. Bodinier (1996), Origin of the recrystallisation front in the Ronda peridotite by km-scale pervasive porous melt flow, *Contrib. Mineral. Petrol.*, *122*, 387–405.

Van der Wal, D., and R. L. M. Vissers (1993), Uplift and emplacement of upper mantle rocks in the western Mediterranean, *Geology*, *21*, 1119–1122.

Van der Wal, D., and R. L. M. Vissers (1996), Structural petrology of the Ronda peridotite, SW Spain: Deformation history, *J. Petrol.*, *37*, 23–43.

Vauchez, A., and C. J. Garrido (2001), Seismic properties of an asthenospherized lithospheric mantle: Constraints from lattice preferred orientations in peridotite from the Ronda massif, *Earth Planet. Sci. Lett.*, *192*, 235–249.

Westerhof, A. B. (1977), On the contact relations of high-temperature peridotites in the Serrania de Ronda, southern Spain, *Tectonophysics*, *39*, 579–591.